Targeted Metabolomics Reveals Early Dominant Optic Atrophy Signature in Optic Nerves of *Opa1*$^{delTTAG/+}$ Mice

Juan Manuel Chao de la Barca,[1,2] Gilles Simard,[2,3] Emmanuelle Sarzi,[4] Tanguy Chaumette,[1] Guillaume Rousseau,[2] Stéphanie Chupin,[1,2] Cédric Gadras,[2] Lydie Tessier,[2] Marc Ferré,[1] Arnaud Chevrollier,[1] Valérie Desquiret-Dumas,[1,2] Naïg Gueguen,[1,2] Stéphanie Leruez,[1,5] Christophe Verny,[1,6] Dan Miléa,[1,5,7] Dominique Bonneau,[1,2] Patrizia Amati-Bonneau,[1,2] Vincent Procaccio,[1,2] Christian Hamel,[4] Guy Lenaers,[1] Pascal Reynier,[1,2] and Delphine Prunier-Mirebeau[1,2]

[1]Pôle de Recherche et d'Enseignement en Médecine Mitochondriale (PREMMi), Institut MITOVASC, Université d'Angers, Angers, France
[2]Département de Biochimie et Génétique, Centre Hospitalier Universitaire, Angers, France
[3]Institut National de la Santé et de la Recherche Médicale (INSERM), U1063, Université d'Angers, Angers, France
[4]Institut National de la Santé et de la Recherche Médicale (INSERM), U1051, Institut des Neurosciences de Montpellier, Montpellier, France
[5]Département d'Ophtalmologie, Centre Hospitalier Universitaire, Angers, France
[6]Département de Neurologie, Centre Hospitalier Universitaire, Angers, France
[7]Singapore Eye Research Institute, Singapore National Eye Centre, Duke-NUS, Singapore

Correspondence: Pascal Reynier, Département de Biochimie et Génétique, Centre Hospitalier Universitaire, 4 rue Larrey, Angers, F-49933, France; pareynier@chu-angers.fr.

Submitted: November 15, 2016
Accepted: January 3, 2017

Citation: Chao de la Barca JM, Simard G, Sarzi E, et al. Targeted metabolomics reveals early dominant optic atrophy signature in optic nerves of *Opa1*$^{delTTAG/+}$ mice. *Invest Ophthalmol Vis Sci*. 2017;58:812–820. DOI: 10.1167/iovs.16-21116

Purpose. Dominant optic atrophy (MIM No. 165500) is a blinding condition related to mutations in *OPA1*, a gene encoding a large GTPase involved in mitochondrial inner membrane dynamics. Although several mouse models mimicking the disease have been developed, the pathophysiological mechanisms responsible for retinal ganglion cell degeneration remain poorly understood.

Methods. Using a targeted metabolomic approach, we measured the concentrations of 188 metabolites in nine tissues, that is, brain, three types of skeletal muscle, heart, liver, retina, optic nerve, and plasma in symptomatic 11-month-old *Opa1*$^{delTTAG/+}$ mice.

Results. Significant metabolic signatures were found only in the optic nerve and plasma of female mice. The optic nerve signature was characterized by altered concentrations of phospholipids, amino acids, acylcarnitines, and carnosine, whereas the plasma signature showed decreased concentrations of amino acids and sarcosine associated with increased concentrations of several phospholipids. In contrast, the investigation of 3-month-old presymptomatic *Opa1*$^{delTTAG/+}$ mice showed no specific plasma signature but revealed a significant optic nerve signature in both sexes, although with a sex effect. The *Opa1*$^{delTTAG/+}$ versus wild-type optic nerve signature was characterized by the decreased concentrations of 10 sphingomyelins and 10 lysophosphatidylcholines, suggestive of myelin sheath alteration, and by alteration in the concentrations of metabolites involved in neuroprotection, such as dimethylarginine, carnitine, spermine, spermidine, carnosine, and glutamate, suggesting a concomitant axonal metabolic dysfunction.

Conclusions. Our comprehensive metabolomic investigations revealed in symptomatic as well as in presymptomatic *Opa1*$^{delTTAG/+}$ mice, a specific sensitiveness of the optic nerve to Opa1 insufficiency, opening new routes for protective therapeutic strategies.

Keywords: dominant optic atrophy, optic neuropathy, *OPA1*, metabolomics, mitochondria

Dominant optic atrophy (DOA, MIM No 165500), a blinding mitochondrial disease with a prevalence of 1/35,000 in the general population,[1] is associated with chronic neurodegeneration of the retinal ganglion cells (RGCs) forming the optic nerves. In most cases, DOA appears as an isolated clinical condition with bilateral visual impairment occurring progressively during the first 2 decades of life,[2,3] essentially in relation to dominant haploinsufficient *OPA1* mutations.[4–6] However, approximately 20% of the *OPA1* patients develop additional extraocular neurologic features such as sensorineural deafness, ataxia, peripheral neuropathy, encephalopathy, and myopathy.[7] These syndromic "DOA+" forms (MIM No. 125250) are mostly associated with missense dominant negative *OPA1* mutations.[8–11] In addition, biallelic *OPA1* mutations have recently been described in an early severe Behr-like syndrome (MIM No. 210000), associating severe optic atrophy with spinocerebellar degeneration, pyramidal signs, peripheral neuropathy, gastrointestinal dysmobility, and retarded development,[12–15] and in a recessive syndrome associating optic neuropathy, cardiomyopathy, and encephalopathy.[16] *OPA1* mutations have also been occasionally associated with spastic paraplegia, multiple sclerosis–like and syndromic parkinsonism and dementia.[7,17–19]

The *OPA1* gene, located in 3q28-q29, comprises 30 coding exons, and encodes a ubiquitously expressed dynamin-related GTPase anchored to the mitochondrial inner membrane facing the intermembrane space.[20,21] OPA1 oligomers, which act on mitochondrial inner membrane dynamics allowing structuration of the cristae and fusion of the mitochondrial network,[22] are consequently related to the processes of apoptosis, mitochondrial quality control, mitophagy, and mitochondrial DNA maintenance and distribution.[23–25]

From a pathophysiological point of view, investigations of the skeletal muscle of *OPA1* patients have revealed multiple deletions of the mitochondrial DNA (mtDNA), confirming the involvement of OPA1 in mtDNA maintenance.[8,9] Explorations of *OPA1* cell models have further revealed altered oxidative phosphorylation (OXPHOS), excitotoxicity, oxidative stress,[26–30] and modified calcium fluxes.[31,32] Neuronal cell models have also revealed the role of Opa1 in synaptic maturation and dendritic growth.[33] Three different *Opa1*$^{+/-}$ mouse models have been characterized.[34–36] They all present at ~50% reduction of Opa1 protein expression and replicate the human clinical condition, that is, a slowly progressive bilateral optic neuropathy associated with the loss of RGCs. One of these mouse models presents a DOA phenotype with mild extraocular features, including subtle neurologic and metabolic abnormalities,[37] late-onset cardiomyopathy,[38] and increased endurance.[39] The *Opa1*$^{delTTAG/+}$ mouse model that we have developed presents a multisystemic neurodegenerative DOA+ phenotype associating optic atrophy, deafness, encephalomyopathy, peripheral neuropathy, and ataxia.[40] Further characterization of these models reveals altered RGC myelination, abnormal dendritogenesis[41] as well as increased numbers of mitophagic vesicles.[40] We also have found a complex IV defect specifically in the retina, optic nerve, and glycolytic muscle fibers.

Although these studies evidence alterations of RGC survival and functionality, no connection has been established so far between OPA1 dysfunction and the general cell metabolism, in particular that of phospholipids, amino acids, biogenic amines, and acylcarnitines. To address this question, we conducted a comprehensive targeted metabolomic and lipidomic study, measuring 188 metabolites by using mass spectrometry in nine tissues, that is, brain, three types of skeletal muscle, heart, liver, retina, optic nerve, and plasma, of symptomatic and presymptomatic *Opa1*$^{+/-}$ mice and controls, cumulating more than 70,000 metabolite measurements, which disclosed specific optic nerve signature anticipating its dysfunction and degeneration.

Methods

Animals and Sampling Procedures

All experiments were performed in accordance with the European Community Guiding Principles for the care and use of animals (Directive 2010/63/UE; Décret No. 2013-118) and in accordance to the ARVO Statement for the Use of Animals in Ophthalmic and Vision Research. Details of the construction of the *Opa1*$^{delTTAG/+}$ mouse model and the phenotypic characterization have been previously published.[36,40] Our metabolomic analysis was carried out on a total of 75 *Opa1*$^{delTTAG/+}$ and control mice divided into two groups, one composed of 40 3-month-old (3-Mo) mice and the other of 35 11-month-old (11-Mo) mice. All animals were maintained in a room at constant temperature (21°C ± 2°C) with a 12-hour light/dark cycle, and given free access to standard chow and water. Euthanasia by decapitation and tissue sampling were always performed by the same trained operators, at the same time of day after administration of volatile anesthesia (isoflurane), in order to optimize the homogeneity of the sampling procedure. Immediately after culling, blood was collected from 3-Mo and 11-Mo mice by using heparinized syringes and centrifuged at 5000*g* for 5 minutes at +4°C, the plasma being recovered and immediately stored at −80°C until analysis. Samples of the optic nerve, retina, brain, heart, skeletal muscles, and liver of 11-Mo mice, and of the optic nerve alone of 3-Mo mice, were immediately stored at −80°C until the extraction of metabolites. Three types of skeletal muscle were studied, that is, the soleus, gluteus maximus, and gastrocnemius, each of them having different proportions of oxidative and glycolytic fibers. Six other *Opa1*$^{delTTAG/+}$ mice, three of which were 4-Mo wild-type mice and three of which were 9-Mo Opa1$^{+/-}$ mice, were used for electron microscopy examination.

Processing Samples for Metabolomic Analysis

The protocols of sample processing and metabolite extraction from brain, liver, heart, gluteus maximus, and gastrocnemius were adapted by calculating the volume of the solvent used for extracting metabolites on the basis of sample weight, as described elsewhere (Application note 1004-1, Biocrates, Bogumil, R. 2009; http://www.biocrates.com/images/stories/pdf/biocrates_appl.note_1004-1.pdf; in the public domain). In brief, tissue samples were collected in precooled (dry ice) 2.0-mL homogenization Precellys tubes prefilled with 1.4-mm-diameter ceramic beads and cold methanol (6 µL/mg tissue for liver samples and 3 µL/mg tissue for brain, heart, gluteus maximus, and gastrocnemius). Tissues were homogenized with two grinding cycles, each at 6600 rpm for 20 seconds, spaced by 20 seconds, using a Precellys homogenizer (Bertin Technologies, Montigny-le-Bretonneux, France) kept in a room at +4°C. The supernatant was recovered after centrifuging the homogenate and kept at −80°C until mass spectrometric analysis. For the smaller samples, that is, retina, optic nerve, and soleus, the protocol was slightly modified in order to enhance recovery of metabolites. Retina, optic nerve, and soleus samples were placed in 0.5-mL precooled Precellys tubes prefilled with 1.4-mm-diameter ceramic beads; 175 µL cold mixture of methanol and water (140:35 vol/vol) was added and the tissues were homogenized as indicated above. After centrifugation at 16,000*g* for 5 minutes, 140 µL supernatant was transferred to an Eppendorf tube for spin-drying. The samples extracted were kept at −80°C until metabolomic analysis.

Metabolomic Analysis

We applied a targeted, quantitative metabolomic approach to plasma and tissue extracts by using the Biocrates AbsoluteIDQ p180 Kit (Biocrates Life Sciences AG, Innsbruck, Austria). This kit, in combination with an AB Sciex QTRAP 5500 (SCIEX, Villebon sur Yvette, France) mass spectrometer, enables quantification of up to 188 different endogenous molecules, including 40 acylcarnitines, 21 amino acids, 21 biogenic amines, 90 glycerophospholipids, 15 sphingolipids, and 1 "hexose." Supplementary Table S1 shows a complete list of the metabolites measured. Flow-injection analysis with tandem mass spectrometry (FIA-MS/MS) was used for quantifying acylcarnitines, glycerophospholipids, sphingolipids, and sugars, whereas liquid chromatography (LC) allowed the separation of amino acids and biogenic amines before detection with tandem mass spectrometry (LC-MS/MS). Samples were prepared according to the Biocrates Kit User Manual. In brief, after thawing on ice, 10 µL of each sample (tissue homogenate supernatant or plasma) was added to the center of the filter placed on the upper wall of the well in a 96-well plate. Dry extracts from the retina, optic

nerve, and soleus were resuspended in 30 μL methanol, and after thorough vortexing, 10 μL were placed on the top filter. Metabolites were extracted in a methanol solution by using ammonium acetate after drying the filter spot under nitrogen flow and derivatizing with phenylisothiocyanate for the quantification of amino acids and biogenic amines. Extracts were finally diluted with MS running the solvent before FIA and LC-MS/MS analyses. After validation of the three levels of quality control used with the kit, the metabolite concentrations inferred were used for statistical analyses.

Statistical Analyses

For statistical analyses, only metabolites with more than 70% of their concentration values in the dynamic range were taken into consideration. Data from the retina, optic nerve, and soleus were analyzed as compositional data, fixing the sum of the whole set of metabolites per sample at unit value. This was done to minimize the between-sample differences in metabolite concentration due merely to differences in the amount of tissue extracted. The nonparametric Wilcoxon rank sum test was used for group comparisons involving quantitative variables. Differences were considered statistically significant at $P \leq 0.05$, unless otherwise mentioned. Univariate analyses were conducted by using R software, version 3.1.1 (The R Foundation for Statistical Computing, Vienna, Austria).

Multivariate analysis was performed by using unit variance-scaled data. Principal component analysis (PCA) was used to detect strong outliers and similar samples forming clusters. A supervised method called orthogonal projection to latent structures by means of partial least square–discriminant analysis, or OPLS-DA, was used to find the linear combination of metabolite concentration in the X (matrix of metabolite) space that correlates the best with the Y vector of responses (wild type/*Opa1*$^{+/-}$). When Y is not a vector but a matrix containing, for example, two response variables, such as sex and genotype, this method is called O2PLS-DA. The quality of models was appreciated by using two parameters: R^2 (goodness of fit) and Q^2_{cum} (goodness of prediction). In the model with the best predictive capabilities (i.e., $Q^2_{cum} > 0.5$), the risk of overfitting was measured by the predictive capabilities ($Q^2_{cum\text{-}perm}$) of the model obtained when elements of the response vector Y (Y_{perm}) were randomly permuted (permutation test). A nonoverfitted model is characterized by poor predictive capabilities (i.e., negative $Q^2_{cum\text{-}perm}$) when the permutation test yields models with no correlation between Y and Y_{perm}. In the model retained, the variables, that is, the metabolites, were selected according to their variable influence for the projection (VIP) and their loading scaled as a correlation coefficient (p_{cor}) between the original variable in the X matrix and the predictive component of interest. For a variable m, and a unique predictive component tp, VIP_m summarizes its importance for the OPLS-DA model, whereas $p_{cor,m}$ indicates the magnitude of the correlation between m and tp. Thus, important variables (i.e., VIP > 1) having a high absolute p_{cor} value were retained, since they were considered to be critical for group discrimination in predictive models. Plotting the VIP value versus p_{cor} for all variables (the "volcano" plot) enables ready visualization of the importance of each variable for group discrimination in the OPLS model. Multivariate data analysis was carried out by using the SIMCA-P software 14.0 (Umetrics, Umeå, Sweden).

Electron Microscopy Assessment of Optic Nerve Ultrastructure

Optic nerves were dissected and fixed in 2.5% glutaraldehyde in 0.1 M, pH 7.3, phosphate-buffered saline. Thin sections (85 nm, Leica-Reichert Ultracut E; Leica Microsystems, Nanterre, France, were collected and counterstained with uranyl acetate (1.5% in EtOH 70%) and observed with a Hitachi 7100 transmission electron microscope Hitachi, Velizi, France.

Table. Age and Weight Distribution of 3-Month-Old and 11-Month-Old Wild-Type and *Opa1*$^{+/-}$ Mice

Genotype	Sex	Age, d	Weight, g
3-mo mice, $n = 40$			
Wild type, $n = 20$	Male, $n = 10$	97.8 ± 2.35	27.5 ± 0.80
	Female, $n = 10$	97.8 ± 1.53	21.8 ± 0.48
Opa1$^{+/-}$, $n = 20$	Male, $n = 10$	97.7 ± 1.83	27.9 ± 0.76
	Female, $n = 10$	100.5 ± 0.78	22.1 ± 0.39
11-mo mice, $n = 35$			
Wild type, $n = 16$	Male, $n = 7$	334.4 ± 2.23	35.6 ± 1.64
	Female, $n = 9$	328.0 ± 2.64	27.4 ± 1.24
Opa1$^{+/-}$, $n = 19$	Male, $n = 11$	330.6 ± 2.06	34.1 ± 1.56
	Female, $n = 8$	335.1 ± 4.01	26.8 ± 1.63

Data are provided as mean ± standard errors.

Results

We carried out metabolomic studies on 75 *Opa1*$^{delTTAG/+}$ mice, 35 from the 11-Mo group and 40 from the 3-Mo group. The Table shows the distribution of the age and weight of the mice according to sex and *Opa1* genotype.

The Weight of *Opa1*$^{delTTAG/+}$ Mice Depends on the Sex but Not on the Genotype

At the age of 3 months, the weight of males was significantly higher than that of females in wild-type and *Opa1*$^{+/-}$ groups ($P = 1.90*10^{-5}$ and $P = 1.18*10^{-5}$, respectively). This sexual dimorphism of weight was also observed in wild-type and *Opa1*$^{+/-}$ groups at the age of 11 months ($P = 0.024$ and $P = 0.005$, respectively), without evidencing influence of *Opa1* genotype on weight. Eleven-month-old male and female mice had higher weights than 3-Mo wild-type and *Opa1*$^{+/-}$ mice ($P = 2.19*10^{-4}$ and $P = 6.87*10^{-5}$, respectively). The factors controlled in this study were the age at the date of euthanasia, as well as the sex and the genotype of the mice.

Specific Sex-Dependent Metabolomic Signatures in the Optic Nerve and Plasma of Symptomatic 11-Mo Mice

After validation of the quality controls and inclusion of all tissue sample data in the multivariate analysis, using the OPLS-DA algorithm, we found a good discrimination between male and female samples, both in the wild-type and *Opa1*$^{+/-}$ mice, in liver, heart, gastrocnemius, soleus, and gluteus maximus samples (data not shown). Unsupervised PCA showed no strong outliers and no clustering according to *Opa1* genotype, and we could not find a significant OPLS-DA model ($Q^2 < 0.5$) for discriminating *Opa1*$^{+/-}$ mice from controls, for any of the tissues analyzed (data not shown). When *Opa1*$^{+/-}$ mice were compared to controls according to sex, a significant separation was found only in the optic nerve and plasma. Indeed, OPLS-DA models discriminating between wild-type and *Opa1*$^{+/-}$ females led to relevant predictive capabilities for the plasma ($Q^2_{cum} = 0.57$; Fig. 1A for PCA, Fig. 1B for OPLS-DA) and optic nerve ($Q^2_{cum} = 0.52$; Fig. 1D for PCA, Fig. 1E for OPLS-DA). The risk of overfitting for both models was evaluated after 800 random permutations of the Y vector at $Q^2_{cum\text{-}perm} = -0.49$ and

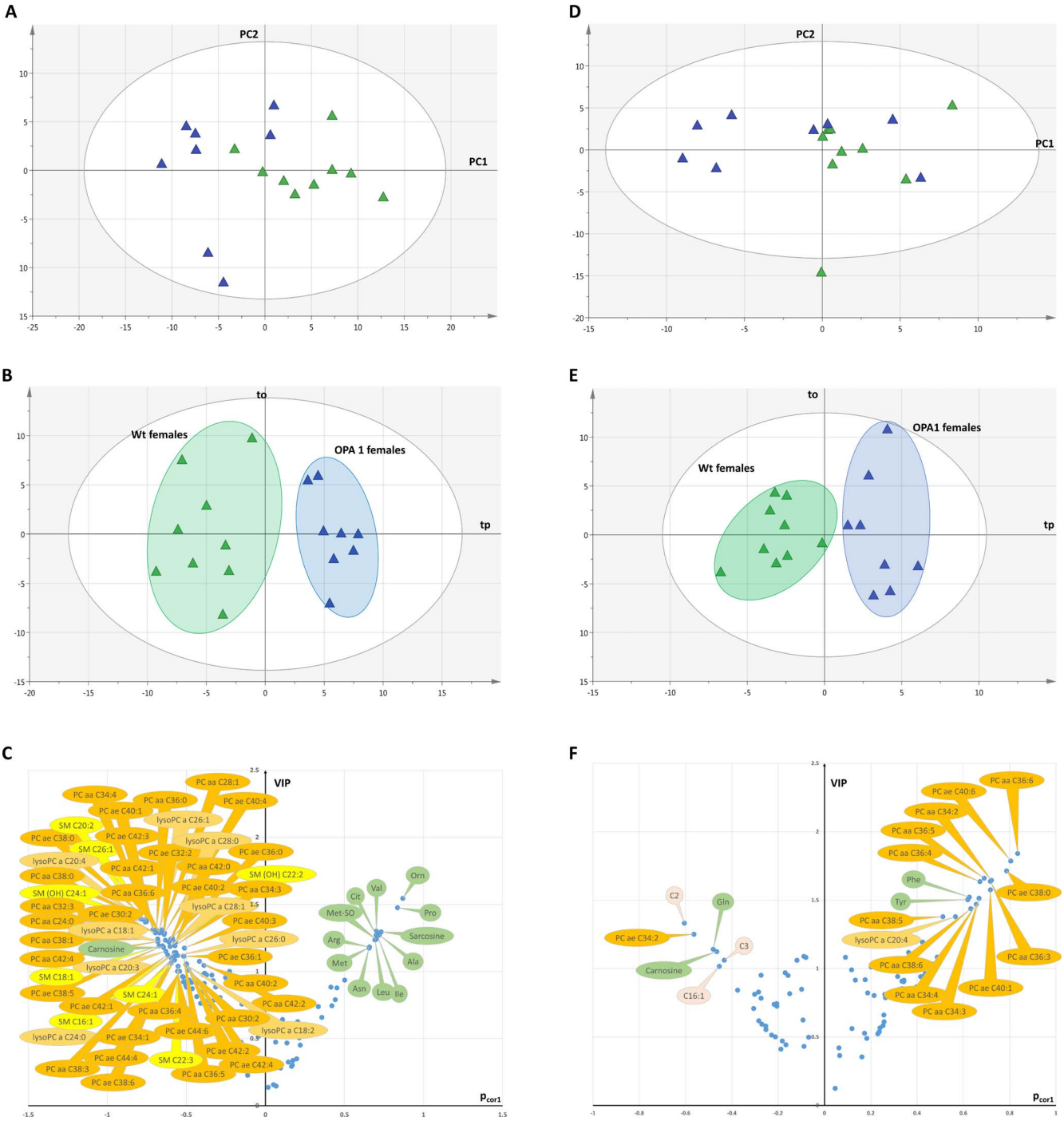

Figure 1. Metabolomic analyses of plasma (**A**–**C**) and the optic nerve (**D**–**F**) of 11-Mo *Opa1*$^{+/-}$ and control female mice. (**A**, **D**) Principal component analysis scatter plots. (**B**, **E**) OPLS-DA scatter plots. (**C**, **F**) Volcano plots (p_{cor} versus VIP). In the volcano plots, amino acids and biogenic amines are represented in *green bubbles*, sphingomyelins in *yellow bubbles*, glycerophosphocholines (phosphatidylcholines and lysophosphatidylcholines) in *dark* and *light orange bubbles*, and acylcarnitines in *pink bubbles*. Ala, alanine; Arg, arginine; Asn, asparagine; Cit, citrulline; C2, acetylcarnitine; C3, propionylcarnitine; C16:1, hexadecenoyl-carnitine; Gln, glutamate; Ile, isoleucine; Leu, leucine; lysoPC a CX:Y, lysophosphatidylcholine acyl; Met, methionine; Met-SO, methionine sulfoxide; Orn, ornithine; PC aa CX:Y, phosphatidylcholine diacyl; PC ae CX:Y, phosphatidylcholine acyl-alkyl; Phe, phenylalanine; Pro, proline; SM CX:Y, sphingomyelin; SM (OH) CX:Y, hydroxysphingomyelin; Tyr, tyrosine; Val, valine. X and Y represent the length of the acyl chain and the number of double bonds, respectively.

$Q^2_{cum\text{-}perm} = -0.50$, respectively. The distribution of metabolites retained in each tissue for statistical analysis is detailed in Supplementary Table S2 for the plasma and Supplementary Table S3 for the optic nerve.

The most discriminant metabolites contributing to these models are presented in the volcano plots (Figs. 1C, 1F). The female-specific plasmatic signature (Fig. 1C) showed the increased concentration of 10 amino acids, that is, ornithine, proline, valine, citrulline, arginine, methionine, alanine, leucine, isoleucine, and asparagine, along with methionine sulfoxide and sarcosine in *Opa1*$^{+/-}$ compared to wild-type mice. Conversely, the concentrations of 53 lipids (phosphati-

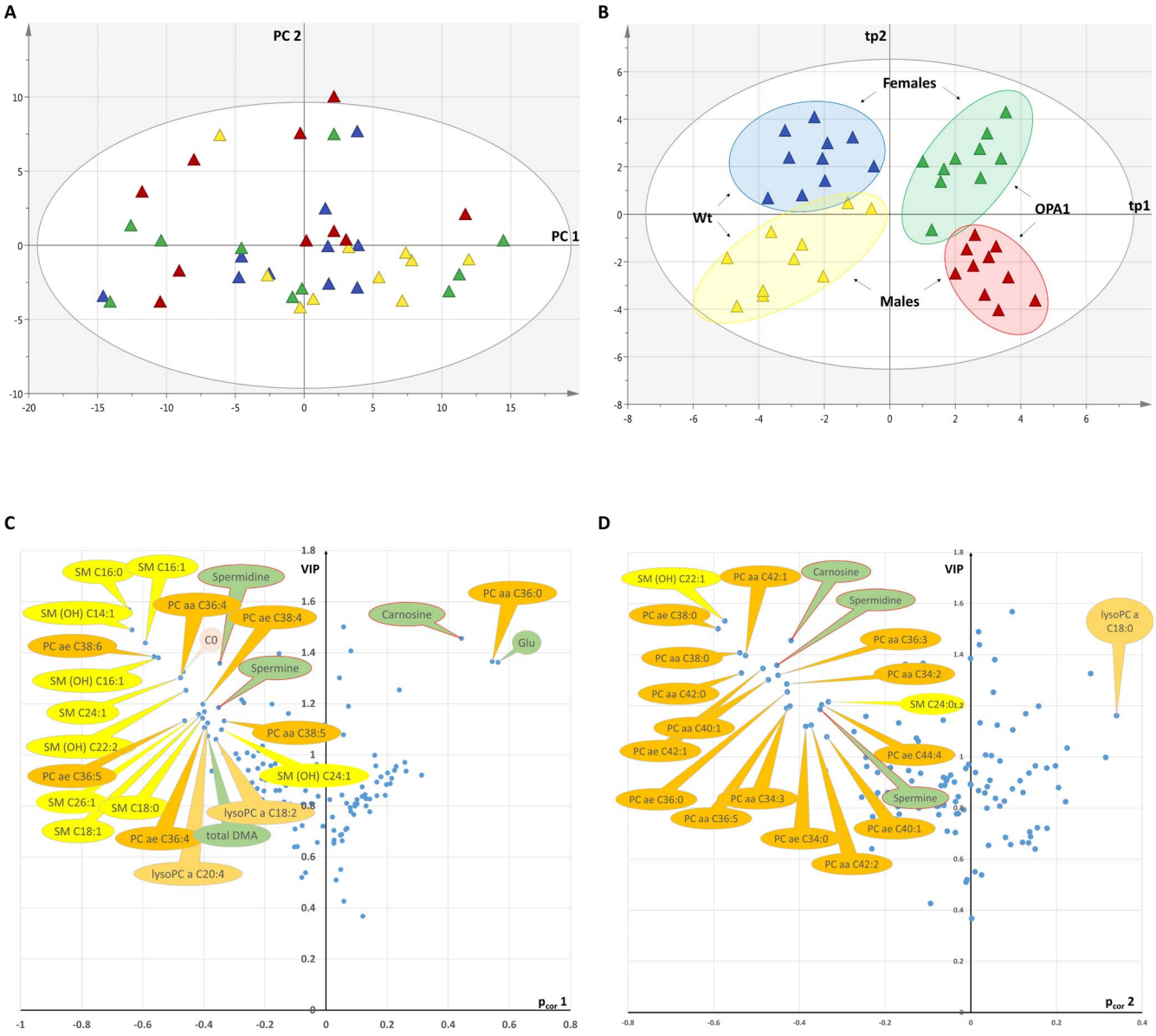

Figure 2. Metabolomic analysis of the optic nerve in 3-Mo *Opa1*$^{+/-}$ mice and control male and female mice. (**A**) Principal component analysis scatter plot. (**B**) OPLS-DA scatter plot. (**C**, **D**) Volcano plots of the OPLS-DA model for the main metabolites discriminating between *Opa1*$^{+/-}$ mice optic nerves according to *Opa1* genotype (**C**) or sex (**D**). Metabolites with negative p_{cor} values (on the *left side* of the volcano plots) in (**C**) and (**D**) show reduced concentrations in *Opa1*$^{+/-}$ mice and in the optic nerves of female mice, respectively. Glutamate (Glu) and biogenic amines are represented in *green bubbles*, carnitine (C0) in a *pink bubble*, sphingomyelins in *yellow bubbles*, and glycerophosphocholines, that is, phosphatidylcholines and lysophosphatidylcholines, in *dark* and *light orange bubbles*, respectively. The main metabolites for both signatures are framed in *red*. Total DMA, total dimethylarginine. X and Y represent the length of the acyl chain and the number of double bonds, respectively.

dylcholines, lysophosphatidylcholines, and sphingomyelins) and carnosine were decreased in the plasma of *Opa1*$^{+/-}$ as compared to wild-type female mice. The optic nerve (Fig. 1F) of female *Opa1*$^{+/-}$ mice showed increased concentrations of 13 phosphatidylcholines and 2 aromatic amino acids (phenylalanine and tyrosine) and decreased concentrations of 3 acylcarnitines (acetyl-, propionyl- and hexadecenoyl-carnitine), glutamate, carnosine, and phosphatidylcholine PC ae 34:2.

Discriminant Signatures in the Optic Nerve of Presymptomatic 3-Mo Mice of Both Sexes Accompanied by a Sex Effect

Data showing a specific metabolomics signature in the optic nerve and plasma of 11-Mo female mice prompted us to consider these data in presymptomatic 3-Mo animals. In the 3-Mo group, there was no distinction between *Opa1*$^{+/-}$ and wild-type plasma samples ($Q^2 < 0.5$), conversely to the one found in 11-Mo females. There was no outlier in the PCA of the optic nerve data, nor clustering according to the *Opa1* genotype (Fig. 2A), and the OPLS-DA algorithm yielded a model with good predictive capabilities ($Q^2 = 0.51$). In this model, discrimination between *Opa1*$^{+/-}$ mice and wild-type mice was achieved in the first predictive component, tp1, while the second orthogonal predictive component tp2 distinguished male from female mice (Fig. 2B). The risk of overfitting was evaluated at $Q^2_{cum\text{-}perm} = -0.57$ after 800 random permutations of the two Y vectors. The most discriminant metabolites contributing to these models are presented as volcano plots (Figs. 2C, 2D). The *Opa1*$^{+/-}$–related signature (Fig. 2C) was

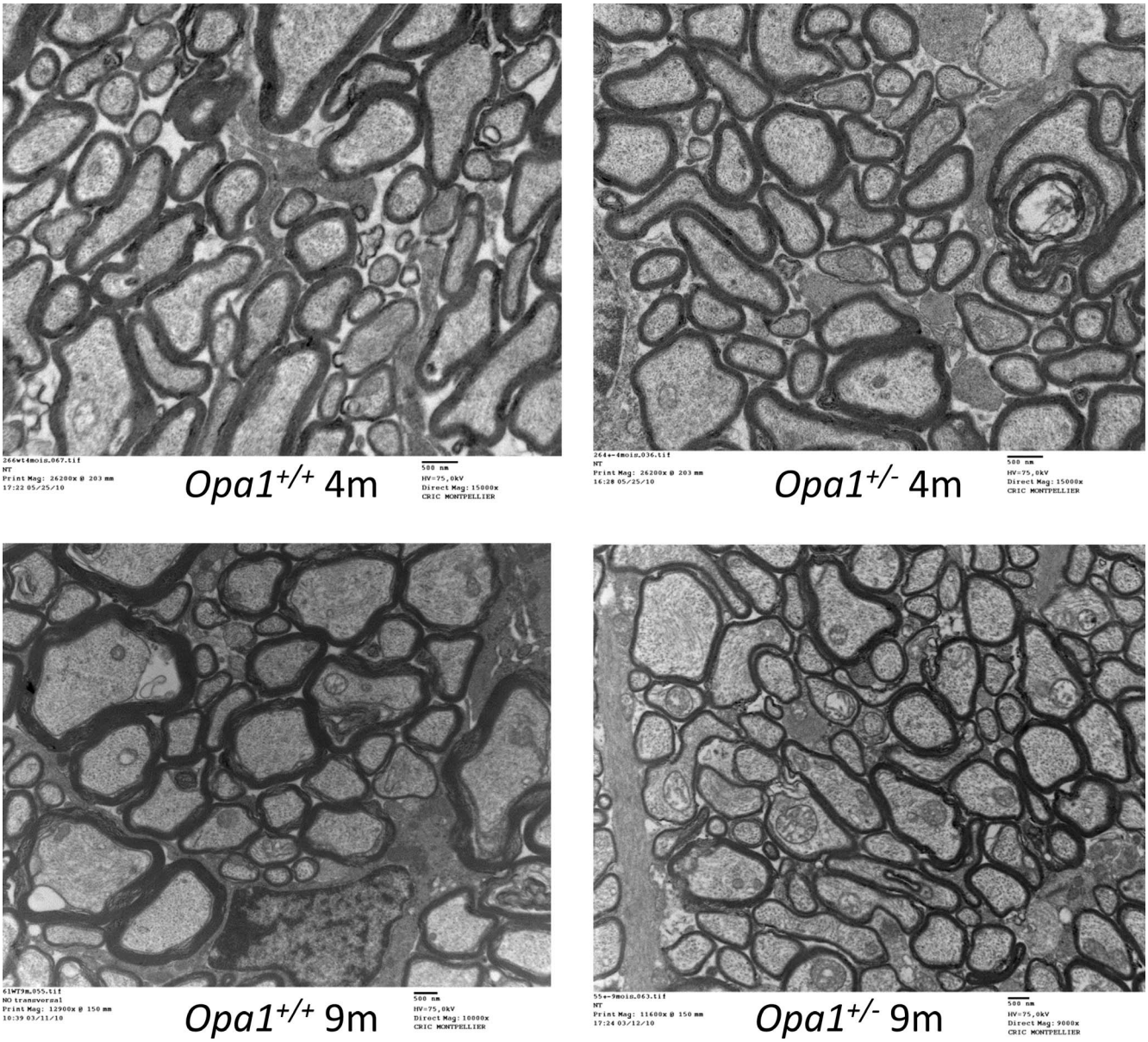

FIGURE 3. Electron microscopy of optic nerve cross-sections. Pictures of the optic nerve from 4-month-old (*top*) and 9-month-old (*bottom*) wild-type (*left*) and *Opa1*$^{+/-}$ (*right*) mice show reduced myelin sheath thickness specifically in 9-Mo *Opa1*$^{+/-}$ animals.

characterized by the decreased concentrations of 10 sphingomyelins and 10 phosphatidylcholines, carnitine, total dimethylarginine, spermine, and spermidine, and by the increased concentration of glutamate and carnosine in *Opa1*$^{+/-}$ optic nerves compared to controls. The sex-specific signature (Fig. 2D) was characterized by the decreased concentrations of 16 phosphatidylcholines, 2 sphingomyelins, carnosine, spermidine, and spermine, and by the increased concentration of 1 lysophosphatidylcholine, in female mice compared to males.

The existence of a metabolic impairment in both sexes at 11 months cannot be ruled out. Indeed, the size of the optic nerve decreases with age, together with a parallel decrease in the measured concentration of metabolites. In our study, metabolites with concentrations below the lower limit of quantitation for a given proportion of samples were excluded from the statistical analysis. Thus, 132 metabolites were considered to be measured with sufficient accuracy in the optic nerves of 3-Mo *Opa1*$^{+/-}$ mice, whereas only 89 metabolites in the optic nerves of 11-Mo *Opa1*$^{+/-}$ mice were retained for analysis. This weaker number of measurable metabolites at 11-Mo may explain the absence of discriminant model affecting both sexes.

Absence of Ultrastructural Abnormalities in the Optic Nerves of Presymptomatic 4-Mo *Opa1*$^{+/-}$ Mice

There were no noticeable anomalies in the optic nerve ultrastructure of 4-Mo *Opa1*$^{+/-}$ mice compared to controls (Fig. 3, top). This is consistent with the absence of functional impairment of vision observed at this age.[40] In contrast, in 9-Mo *Opa1*$^{+/-}$ mice, when the visual functionality is altered, a sharp reduction in the thickness of the axonal myelin sheath was observed together with intra-axonal mitochondrial swelling (Fig. 3, bottom) as already reported for this model at 16 months of age.[40]

Discussion

Although less exhaustive than the untargeted metabolomics, the targeted metabolomics used in this study have the advantage of providing quantitative or semiquantitative measurements of metabolite concentrations. The Biocrates AbsoluteIDQ p180 Kit integrates calibration curves and several quality controls, allowing well-controlled measurements and reproducibility. The panel of metabolites analyzed with this kit (Supplementary Table S1) also offers the advantage of combining both polar and lipid metabolites, allowing a large overview of metabolic pathways. To investigate the overall metabolic consequences of Opa1 haploinsufficiency, we analyzed with this kit 188 metabolites in nine tissues of 35 11-Mo mice.

The comparison between *Opa1*$^{+/-}$ and *Opa1*$^{+/+}$ mice showed no significant difference of metabolic profile in the retina, brain, gastrocnemius, gluteus maximus, soleus, heart, and liver. This rather surprising finding suggests that discriminant Opa1-related metabolites may not have been represented among the metabolites we targeted, or that *Opa1* haploinsufficiency leads to only minor, undetectable metabolic consequences in these tissues. Since significant metabolomic signatures were identified only in the optic nerve and plasma of 11-Mo symptomatic female *Opa1*$^{+/-}$ mice, we carried out a further study of the optic nerve and plasma of 3-Mo presymptomatic *Opa1*$^{+/-}$ mice. At this age, an *Opa1*-related optic nerve metabolic signature, affecting both females and males, was found, although with evidence of sexual dimorphism, whereas the plasma showed no significant alteration of the metabolomic profile.

The sex effect of OPA1 deficiency that we observed is quite unexpected. We recently have observed in our *Opa1*$^{+/-}$ mouse model a significant increase of pregnenolone and 17-β-estradiol in the blood and retina of female mice.[36] These female *Opa1*$^{+/-}$ mice display an earlier and more exacerbated RGC degeneration than males, these differences being abolished by ovariectomy. Thus, the metabolomic sex effect we found in the optic nerve and plasma may be related to the increased steroid background in female *Opa1*$^{+/-}$ mice. Furthermore, we have found that women show worse vision loss at adolescence and greater decrease in retinal nerve fibers than men.[36]

We previously have shown that the optic atrophy in this mouse *Opa1*$^{+/-}$ model begins to be perceptible at approximately 5 to 6 months and progressively increases, as attested by the alteration of the visual evoked potential and the decline of the RGC count measured by immunohistochemistry.[40] The metabolites, being reduced in the optic nerve of 3-Mo *Opa1*$^{+/-}$ mice before the loss of RGCs, may be intimately related to the mechanism underlying optic nerve degeneration. The decreased concentration of sphingomyelins and phosphatidylcholines are likely to reflect an alteration of the myelin sheath as an early pathophysiological event, the sphingomyelins being the main constituents of the myelin sheath surrounding the axons. The distinct reduction of myelin sheath thickness accompanying the optic neuropathy in 9-Mo *Opa1*$^{+/-}$ mice is consistent with the degeneration of myelin although the reduction in thickness was not visible in the 4-Mo *Opa1*$^{+/-}$ mice examined by electron microscopy.

Six polar metabolites also contribute to the optic nerve signature in 3-Mo *Opa1*$^{+/-}$ mice, with decreased carnitine, total dimethylarginine, spermine, and spermidine, and increased glutamate and carnosine. The brain has the highest levels of polyamines such as spermine and spermidine. A study on goldfish has revealed that spermidine and spermine are actively transported in the axons of optic nerves.[42] Spermidine, which mediates protection against oxidative damage, has a neuroprotective effect on RGCs in adult mice after optic nerve injury[43] and prevents RGC neurodegeneration in a mouse model of normal tension glaucoma.[44] Asymmetric dimethylarginine is an endogenous inhibitor of nitric oxide synthase (NOS), while symmetric dimethylarginine is a competitive inhibitor of the cellular uptake of L-arginine, the substrate for NOS. These two metabolites underscore the potential role of the nitric-oxide (NO) pathway in DOA pathogenesis, NO being involved in neuroprotection through vasodilatation and antioxidative effects. Similarly, carnitine is neuroprotective because of its antioxidant and antiapoptotic activities in the optic nerve and RGCs.[45] Carnitine has also a neuroprotective and antioxidant action in an experimental rat model of glaucoma.[46] Glutamate, the main excitatory neurotransmitter in the retina, is well known to be toxic when present in excessive amounts as found in the metabolic signature we reported here. Carnosine, which is also increased in the signature, is a dipeptide composed of alanine and histidine, which exerts several biological effects including antioxidant action.[47] Its intravitreal injection is neuroprotective for RGCs, following retinal injury.[48] The action of carnosine may be further linked to that of glutamate, since carnosine decreases neuronal cell death by targeting the glutamate system.[49] The increased carnosine in our signature may be interpreted as a mechanism aimed at counteracting the increased excitatory glutamate concentration. Thus, the six polar metabolites with modified concentrations in the optic nerve of *Opa1*$^{+/-}$ mice, that is, carnitine, dimethylarginine, spermine, spermidine, glutamate, and carnosine, are promising candidates for explaining the presymptomatic RGC axonal dysfunction observed in OPA1 and its successive degeneration.

In 11-Mo *Opa1*$^{+/-}$ mice, the optic nerve signature was identified only in female mice and was very different from that observed in 3-Mo *Opa1*$^{+/-}$ mice, which involved a smaller number of metabolites. Reduced concentrations of acetylcarnitine, propionylcarnitine, and palmitoleic acid may reflect a late-onset reduced oxidation of carbohydrate and fatty acids, consistent with the OXPHOS defect we observed previously, whereas the large increase of phosphatidylcholines may correspond to the remodeling of the optic nerve and the glial cicatrix that follows the loss of RGCs. In the plasma of 11-Mo female *Opa1*$^{+/-}$ mice, the influence of Opa1 deficiency was marked by the altered concentration of 65 metabolites. The increased plasmatic concentrations of 17β-estradiol and pregnenolone, previously reported in *Opa1*$^{+/-}$ mice,[36] probably explain why Opa1 deficiency produces such high metabolic effects in the plasma of 11-Mo female *Opa1*$^{+/-}$ mice.

Finally, the results of our comprehensive metabolomic study on *Opa1*$^{+/-}$ mice are highly consistent with the pathophysiology of the disease, optic neuropathy being the hallmark of nearly all OPA1-related disorders described so far. Indeed, the optic nerves of *Opa1*$^{+/-}$ mice were specifically affected at the metabolic level, from the age of 3 months onwards with phospholipidic and polar metabolomic signatures, highly suggestive of presymptomatic myelin sheath alteration, excitotoxicity, deficiency of metabolites counteracting oxidative stress, and alteration of the NO pathway.

Acknowledgments

The authors thank Kanaya Malkani for critical reading and comments on the manuscript, and the team of Service Commun d'Animalerie Hospitalo-Universitaire d'Angers.

Supported by INSERM, CNRS, the University of Angers, the University Hospital of Angers, the Région Pays de Loire and Angers Loire Métropole. Supported by grants from the following patients' foundations: Fondation VISIO, Ouvrir les Yeux, Union Nationale des Aveugles et Déficients Visuels, Association contre les Maladies Mitochondriales, Retina France, Kjer France, Fondation Berthe

Fouassier, Fondation pour la Recherche Médicale, and Association Point de Mire.

Disclosure: **J.M. Chao de la Barca**, None; **G. Simard**, None; **E. Sarzi**, None; **T. Chaumette**, None; **G. Rousseau**, None; **S. Chupin**, None; **C. Gadras**, None; **L. Tessier**, None; **M. Ferré**, None; **A. Chevrollier**, None; **V. Desquiret-Dumas**, None; **N. Gueguen**, None; **S. Leruez**, None; **C. Verny**, None; **D. Miléa**, None; **D. Bonneau**, None; **P. Amati-Bonneau**, None; **V. Procaccio**, None; **C. Hamel**, None; **G. Lenaers**, None; **P. Reynier**, None; **D. Prunier-Mirebeau**, None

References

1. Yu-Wai-Man P, Griffiths PG, Burke A, et al. The prevalence and natural history of dominant optic atrophy due to OPA1 mutations. *Ophthalmology*. 2010;117:1538–1546.e1.
2. Milea D, Amati-Bonneau P, Reynier P, Bonneau D. Genetically determined optic neuropathies. *Curr Opin Neurol*. 2010;23: 24–28.
3. Lenaers G, Hamel C, Delettre C, et al. Dominant optic atrophy. *Orphanet J Rare Dis*. 2012;7:46.
4. Delettre C, Lenaers G, Griffoin JM, et al. Nuclear gene OPA1, encoding a mitochondrial dynamin-related protein, is mutated in dominant optic atrophy. *Nat Genet*. 2000;26:207–210.
5. Alexander C, Votruba M, Pesch UE, et al. OPA1, encoding a dynamin related GTPase, is mutated in autosomal dominant optic atrophy linked to chromosome 3q28. *Nat Genet*. 2000; 26:211–215.
6. Ferré M, Caignard A, Milea D, et al. Improved locus-specific database for OPA1 mutations allows inclusion of advanced clinical data. *Hum Mutat*. 2015;36:20–25.
7. Yu-Wai-Man P, Griffiths PG, Gorman GS, et al. Multi-system neurological disease is common in patients with OPA1 mutations. *Brain*. 2010;133:771–786.
8. Amati-Bonneau P, Valentino ML, Reynier P, et al. OPA1 mutations induce mitochondrial DNA instability and optic atrophy 'plus' phenotypes. *Brain*. 2008;131:338–351.
9. Hudson G, Amati-Bonneau P, Blakely EL, et al. Mutation of OPA1 causes dominant optic atrophy with external ophthalmoplegia, ataxia, deafness and multiple mitochondrial DNA deletions: a novel disorder of mtDNA maintenance. *Brain*. 2008;131:329–337.
10. Yu-Wai-Man P, Trenell MI, Hollingsworth KG, Griffiths PG, Chinnery PF. OPA1 mutations impair mitochondrial function in both pure and complicated dominant optic atrophy. *Brain*. 2010;34:e164.
11. Leruez S, Milea D, Defoort-Dhellemmes S, et al. Sensorineural hearing loss in OPA1-linked disorders. *Brain*. 2013;136:e236.
12. Schaaf CP, Blazo M, Lewis RA, et al. Early-onset severe neuromuscular phenotype associated with compound heterozygosity for OPA1 mutations. *Mol Genet Metab*. 2011;103: 383–387.
13. Bonneau D, Colin E, Oca F, et al. Early-onset Behr syndrome due to compound heterozygous mutations in OPA1. *Brain*. 2014;37:e301.
14. Bonifert T, Karle KN, Tonagel F, et al. Pure and syndromic optic atrophy explained by deep intronic OPA1 mutations and an intralocus modifier. *Brain*. 2014;137:2164–2177.
15. Carelli V, Sabatelli M, Carrozzo R, et al. 'Behr syndrome' with OPA1 compound heterozygote mutations. *Brain*. 2015;138: e321.
16. Spiegel R, Saada A, Flannery PJ, et al. Fatal infantile mitochondrial encephalomyopathy, hypertrophic cardiomyopathy and optic atrophy associated with a homozygous OPA1 mutation. *J Med Genet*. 2016;53:127–131.
17. Verny C, Loiseau D, Scherer C, et al. Multiple sclerosis-like disorder in OPA1-related autosomal dominant optic atrophy. *Neurology*. 2008;70:1152–1153.
18. Carelli V, Musumeci O, Caporali L, et al. Syndromic parkinsonism and dementia associated with OPA1 missense mutations. *Ann Neurol*. 2015;78:21–38.
19. Chao de la Barca JM, Prunier-Mirebeau D, Amati-Bonneau P, et al. OPA1-related disorders: diversity of clinical expression, modes of inheritance and pathophysiology. *Neurobiol Dis*. 2016;90:20–26.
20. Olichon A, Emorine LJ, Descoins E, et al. The human dynamin-related protein OPA1 is anchored to the mitochondrial inner membrane facing the inter-membrane space. *FEBS Lett*. 2002; 523:171–176.
21. Olichon A, Guillou E, Delettre C, et al. Mitochondrial dynamics and disease, OPA1. *Biochim Biophys Acta*. 2006; 1763:500–509.
22. Lenaers G, Reynier P, Elachouri G, et al. OPA1 functions in mitochondria and dysfunctions in optic nerve. *Int J Biochem Cell Biol*. 2009;41:1866–1874.
23. Olichon A, Landes T, Arnauné-Pelloquin L, et al. Effects of OPA1 mutations on mitochondrial morphology and apoptosis: relevance to ADOA pathogenesis. *J Cell Physiol*. 2007;211: 423–430.
24. Elachouri G, Vidoni S, Zanna C, et al. OPA1 links human mitochondrial genome maintenance to mtDNA replication and distribution. *Genome Res*. 2011;21:12–20.
25. Belenguer P, Pellegrini L. The dynamin GTPase OPA1: more than mitochondria? *Biochim Biophys Acta*. 2013;1833:176–183.
26. Chevrollier A, Guillet V, Loiseau D, et al. Hereditary optic neuropathies share a common mitochondrial coupling defect. *Ann Neurol*. 2008;63:794–798.
27. Kanazawa T, Zappaterra MD, Hasegawa A, et al. The C. elegans Opa1 homologue EAT-3 is essential for resistance to free radicals. *PLoS Genet*. 2008;4:e1000022.
28. Tang S, Le PK, Tse S, Wallace DC, Huang T. Heterozygous mutation of Opa1 in Drosophila shortens lifespan mediated through increased reactive oxygen species production. *PLoS One*. 2009;4:e4492.
29. Nguyen D, Alavi MV, Kim KY, et al. A new vicious cycle involving glutamate excitotoxicity, oxidative stress and mitochondrial dynamics. *Cell Death Dis*. 2011;2:e240.
30. Millet A, Bertholet A, Daloyau M, et al. Loss of functional OPA1 unbalances redox state: implications in dominant optic atrophy pathogenesis. *Ann Clin Transl Neurol*. 2016;3:408–421.
31. Dayanithi G, Chen-Kuo-Chang M, Viero C, Hamel C, Muller A, Lenaers G. Characterization of Ca2+ signalling in postnatal mouse retinal ganglion cells: involvement of OPA1 in Ca2+ clearance. *Ophthalmic Genet*. 2010;31:53–65.
32. Kushnareva YE, Gerencser AA, Bossy B, et al. Loss of OPA1 disturbs cellular calcium homeostasis and sensitizes for excitotoxicity. *Cell Death Differ*. 2013;20:353–365.
33. Bertholet AM, Millet AM, Guillermin O, et al. OPA1 loss of function affects in vitro neuronal maturation. *Brain*. 2013; 136:1518–1533.
34. Alavi MV, Bette S, Schimpf S, et al. A splice site mutation in the murine Opa1 gene features pathology of autosomal dominant optic atrophy. *Brain*. 2007;130:1029–1042.
35. Davies VJ, Hollins AJ, Piechota MJ, et al. Opa1 deficiency in a mouse model of autosomal dominant optic atrophy impairs mitochondrial morphology, optic nerve structure and visual function. *Hum Mol Genet*. 2007;16:1307–1318.
36. Sarzi E, Seveno M, Angebault C, et al. Increased steroidogenesis promotes early-onset and severe vision loss in females with OPA1 dominant optic atrophy. *Hum Mol Genet*. 2016; 25:2539–2551.
37. Alavi MV, Fuhrmann N, Nguyen HP, et al. Subtle neurological and metabolic abnormalities in an Opa1 mouse model of

Investigative Ophthalmology & Visual Science

autosomal dominant optic atrophy. *Exp Neurol*. 2009;220: 404–409.

38. Chen L, Liu T, Tran A, et al. OPA1 mutation and late-onset cardiomyopathy: mitochondrial dysfunction and mtDNA instability. *J Am Heart Assoc*. 2012;1:e003012.
39. Caffin F, Prola A, Piquereau J, et al. Altered skeletal muscle mitochondrial biogenesis but improved endurance capacity in trained OPA1-deficient mice. *J Physiol*. 2013;591:6017–6037.
40. Sarzi E, Angebault C, Seveno M, et al. The human OPA1delTTAG mutation induces premature age-related systemic neurodegeneration in mouse. *Brain*. 2012;135:3599–3613.
41. Williams PA, Morgan JE, Votruba M. Opa1 deficiency in a mouse model of dominant optic atrophy leads to retinal ganglion cell dendropathy. *Brain*. 2010;133:2942–2951.
42. Ingoglia NA, Sturman JA, Eisner RA. Axonal transport of putrescine, spermidine and spermine in normal and regenerating goldfish optic nerves. *Brain Res*. 1977;130:433–445.
43. Noro T, Namekata K, Kimura A, et al. Spermidine promotes retinal ganglion cell survival and optic nerve regeneration in adult mice following optic nerve injury. *Cell Death Dis*. 2015; 6:e1720.
44. Noro T, Namekata K, Azuchi Y, et al. Spermidine ameliorates neurodegeneration in a mouse model of normal tension glaucoma. *Invest Ophthalmol Vis Sci*. 2015;56:5012–5019.
45. Pescosolido N, Pascarella A, Nebbioso M, Scarsella, G. Degenerative events in retina and optic nerve induced by inhibition of carnitine transport. *J Biol Regul Homeost Agents*. 2014;28:263–270.
46. Calandrella N, De Seta C, Scarsella G, Risuleo G. Carnitine reduces the lipoperoxidative damage of the membrane and apoptosis after induction of cell stress in experimental glaucoma. *Cell Death Dis*. 2010;1:e62.
47. Guiotto A, Calderan A, Ruzza P, Borin G. Carnosine, and carnosine-related antioxidants: a review. *Curr Med Chem*. 2005;12:2293–2231.
48. Russo R, Adornetto A, Cavaliere F, et al. Intravitreal injection of forskolin, homotaurine, and L-carnosine affords neuroprotection to retinal ganglion cells following retinal ischemic injury. *Mol Vis*. 2015;21:718–729.
49. Ouyang L, Tian Y, Bao Y, et al. Carnosine decreased neuronal cell death through targeting glutamate system and astrocyte mitochondrial bioenergetics in cultured neuron/astrocyte exposed to OGD/recovery. *Brain Res Bull*. 2016;124:76–84.

Investigative Ophthalmology & Visual Science